

J. M. Link,<sup>1</sup> P. M. Yager,<sup>1</sup> J. C. Anjos,<sup>2</sup> I. Bediaga,<sup>2</sup> C. Castromonte,<sup>2</sup> A. A. Machado,<sup>2</sup> J. Magnin,<sup>2</sup> A. Massafferri,<sup>2</sup>  
 J. M. de Miranda,<sup>2</sup> I. M. Pepe,<sup>2</sup> E. Polcarpo,<sup>2</sup> A. C. dos Reis,<sup>2</sup> S. Carrillo,<sup>3</sup> E. Casimiro,<sup>3</sup> E. Cuautle,<sup>3</sup>  
 A. Sánchez-Hernández,<sup>3</sup> C. Uribe,<sup>3</sup> F. Vázquez,<sup>3</sup> L. Agostino,<sup>4</sup> L. Cinquini,<sup>4</sup> J. P. Cumalat,<sup>4</sup> B. O'Reilly,<sup>4</sup>  
 I. Segoni,<sup>4</sup> K. Stenson,<sup>4</sup> J. N. Butler,<sup>5</sup> H. W. K. Cheung,<sup>5</sup> G. Chiodini,<sup>5</sup> I. Gaines,<sup>5</sup> P. H. Garbincius,<sup>5</sup>  
 L. A. Garren,<sup>5</sup> E. Gottschalk,<sup>5</sup> P. H. Kasper,<sup>5</sup> A. E. Kreymer,<sup>5</sup> R. Kutschke,<sup>5</sup> M. Wang,<sup>5</sup> L. Benussi,<sup>6</sup> M. Bertani,<sup>6</sup>  
 S. Bianco,<sup>6</sup> F. L. Fabbri,<sup>6</sup> S. Pacetti,<sup>6</sup> A. Zallo,<sup>6</sup> M. Reyes,<sup>7</sup> C. Cawfield,<sup>8</sup> D. Y. Kim,<sup>8</sup> A. Rahimi,<sup>8</sup> J. Wiss,<sup>8</sup>  
 R. Gardner,<sup>9</sup> A. Kryemadhi,<sup>9</sup> Y. S. Chung,<sup>10</sup> J. S. Kang,<sup>10</sup> B. R. Ko,<sup>10</sup> J. W. Kwak,<sup>10</sup> K. B. Lee,<sup>10</sup> K. Cho,<sup>11</sup>  
 H. Park,<sup>11</sup> G. Alimonti,<sup>12</sup> S. Barberis,<sup>12</sup> M. Boschini,<sup>12</sup> A. Cerutti,<sup>12</sup> P. D'Angelo,<sup>12</sup> M. DiCorato,<sup>12</sup> P. Dini,<sup>12</sup>  
 L. Edera,<sup>12</sup> S. Erba,<sup>12</sup> P. Inzani,<sup>12</sup> F. Leveraro,<sup>12</sup> S. Malvezzi,<sup>12</sup> D. Menasce,<sup>12</sup> M. Mezzadri,<sup>12</sup> L. Milazzo,<sup>12</sup>  
 L. Moroni,<sup>12</sup> D. Pedrini,<sup>12</sup> C. Pontoglio,<sup>12</sup> F. Prelz,<sup>12</sup> M. Rovere,<sup>12</sup> S. Sala,<sup>12</sup> T.F. Davenport III,<sup>13</sup> V. Arena,<sup>14</sup>  
 G. Boca,<sup>14</sup> G. Bonomi,<sup>14</sup> G. Gianini,<sup>14</sup> G. Liguori,<sup>14</sup> D. Lopes Pegna,<sup>14</sup> M. M. Merlo,<sup>14</sup> D. Pantea,<sup>14</sup> S. P. Ratti,<sup>14</sup>  
 C. Riccardi,<sup>14</sup> P. Vitulo,<sup>14</sup> C. Göbel,<sup>15</sup> H. Hernandez,<sup>16</sup> A. M. Lopez,<sup>16</sup> H. Mendez,<sup>16</sup> A. Paris,<sup>16</sup> J. Quinones,<sup>16</sup>  
 J. E. Ramirez,<sup>16</sup> Y. Zhang,<sup>16</sup> J. R. Wilson,<sup>17</sup> T. Handler,<sup>18</sup> R. Mitchell,<sup>18</sup> D. Engh,<sup>19</sup> M. Hosack,<sup>19</sup> W. E. Johns,<sup>19</sup>  
 E. Luiggi,<sup>19</sup> J. E. Moore,<sup>19</sup> M. Nehring,<sup>19</sup> P. D. Sheldon,<sup>19</sup> E. W. Vaandering,<sup>19</sup> M. Webster,<sup>19</sup> and M. Sheaff<sup>20</sup>  
 (FOCUS Collaboration)<sup>21</sup>

<sup>1</sup>University of California, Davis, CA 95616

<sup>2</sup>Centro Brasileiro de Pesquisas Físicas, Rio de Janeiro, RJ, Brazil

<sup>3</sup>CINVESTAV, 07000 México City, DF, Mexico

<sup>4</sup>University of Colorado, Boulder, CO 80309

<sup>5</sup>Fermi National Accelerator Laboratory, Batavia, IL 60510

<sup>6</sup>Laboratori Nazionali di Frascati dell'INFN, Frascati, Italy I-00044

<sup>7</sup>University of Guanajuato, 37150 Leon, Guanajuato, Mexico

<sup>8</sup>University of Illinois, Urbana-Champaign, IL 61801

<sup>9</sup>Indiana University, Bloomington, IN 47405

<sup>10</sup>Korea University, Seoul, Korea 136-701

<sup>11</sup>Kyungpook National University, Taegu, Korea 702-701

<sup>12</sup>INFN and University of Milano, Milano, Italy

<sup>13</sup>University of North Carolina, Asheville, NC 28804

<sup>14</sup>Dipartimento di Fisica Nucleare e Teorica and INFN, Pavia, Italy

<sup>15</sup>Pontifícia Universidade Católica, Rio de Janeiro, RJ, Brazil

<sup>16</sup>University of Puerto Rico, Mayaguez, PR 00681

<sup>17</sup>University of South Carolina, Columbia, SC 29208

<sup>18</sup>University of Tennessee, Knoxville, TN 37996

<sup>19</sup>Vanderbilt University, Nashville, TN 37235

<sup>20</sup>University of Wisconsin, Madison, WI 53706

<sup>21</sup>See <http://www-focus.fnal.gov/authors.html> for additional author information.

(Dated: April 27, 2005)

A high statistics measurement of the  $D_s^+$  lifetime from the Fermilab fixed-target FOCUS photoproduction experiment is presented. We describe the analysis of the two decay modes,  $D_s^+ \rightarrow \phi(1020)\pi^+$  and  $D_s^+ \rightarrow \bar{K}^*(892)^0 K^+$ , used for the measurement. The measured lifetime is  $507.4 \pm 5.5$  (stat.)  $\pm 5.1$  (syst.) fs using  $8961 \pm 105$   $D_s^+ \rightarrow \phi(1020)\pi^+$  and  $4680 \pm 90$   $D_s^+ \rightarrow \bar{K}^*(892)^0 K^+$  decays. This is a significant improvement over the present world average.

PACS numbers: 13.25.Ft, 14.40.Lb, 14.65.Dw

Experimental measurements of charm lifetimes have given guidance towards a theoretical description of strong interactions at low energy scales [1, 2]. For example, the ratio of the  $D_s^+$  and  $D^0$  lifetimes gives information on the *weak annihilation* contribution to the total decay [3–6]. Not only is this important for improving our theoretical understanding of strong interactions, but the theoretical tools used to calculate lifetimes are the same or similar to those used in other areas, for example to extract  $|V_{cs}|/|V_{cd}|$  and  $|V_{cb}|$  in charm and bottom decays, or to calculate the  $b$ -particle lifetimes [7, 8].

The data used were collected by the FOCUS collaboration in the 1996–1997 fixed-target run at Fermi National Accelerator Laboratory. The FOCUS spectrometer is an upgrade of the spectrometer used in the E687 photoproduction experiment [9]. In the majority of the data used for this measurement (Run Period *B*) the vertex region consists of four BeO targets and 16 planes of silicon strip detectors (SSD). Two of the SSD planes were placed immediately downstream of the second target, and two immediately downstream of the fourth (most downstream) target. About 20% of the  $D_s^+$  decays used in this anal-

ysis were from data taken earlier in the data-taking run (Run Period A) without the four SSD planes in the target region [10]. Momentum analysis was done using five multiwire proportional chambers and two magnets with opposite polarities. Three multicell threshold Čerenkov counters were used for particle identification [11].

The  $D_s^+ \rightarrow \phi(1020)\pi^+$ ,  $\phi(1020) \rightarrow K^-K^+$  and  $D_s^+ \rightarrow \bar{K}^*(892)^0 K^+$ ,  $\bar{K}^*(892)^0 \rightarrow K^-\pi^+$  resonant decay modes [22] are used because they have much better signal-to-background than inclusive  $D_s^+ \rightarrow K^-K^+\pi^+$  decays.

All  $K^-K^+\pi^+$  candidates are tested to see if they form a vertex with a confidence level greater than 1%. The candidate  $D_s^+$  momentum vector is then projected to search for a production vertex with one or more tracks. As many tracks as possible are included in the production vertex so long as the vertex confidence level is larger than 1%. The production vertex is required to be within one of the four targets. To largely eliminate non-charm backgrounds, the separation  $L$  between the production and decay vertices is required to be larger than  $6\sigma_L$  where  $\sigma_L$  is the calculated error on  $L$ .

The  $\phi(1020)\pi^+$  ( $\bar{K}^*(892)^0 K^+$ ) decay mode candidates are required to have  $K^+K^-$  ( $K^-\pi^+$ ) masses within two sigma of the fitted  $\phi(1020)$  ( $\bar{K}^*(892)^0$ ) mass. Also the magnitude of  $\cos\theta^*$  must be larger than 0.3 (0.6) for the  $\phi(1020)\pi^+$  ( $\bar{K}^*(892)^0 K^+$ ) decay mode candidates, where  $\theta^*$  is the angle between the  $K^-$  and the  $\pi^+$  ( $K^+$ ) in the  $\phi(1020)$  ( $\bar{K}^*(892)^0$ ) center-of-mass frame. For the  $\bar{K}^*(892)^0 K^+$  decay mode, the  $K^+K^-$  invariant mass must not be within two sigma of the  $\phi(1020)$  mass to ensure statistically independent samples in the two decay modes. Each track in the  $K^-K^+\pi^+$  candidate combination must also satisfy a minimal Čerenkov particle identification criteria. To further reduce the  $D^+ \rightarrow K^-\pi^+\pi^+$  contamination by an additional factor of 15 in the  $D_s^+ \rightarrow \bar{K}^*(892)^0 K^+$  candidate sample, the kaon with the same sign as the pion is required to have a kaon probability that is larger than its pion probability by a factor of  $e^3$  [11].

The  $K^-K^+\pi^+$  invariant mass plots for data are shown in Fig. 1. The fits shown are to a Gaussian signal and a quadratic background function which yields  $8961 \pm 105$   $\phi(1020)\pi$  and  $4860 \pm 90$   $\bar{K}^*(892)^0 K$  reconstructed  $D_s^+$  decays. The lifetime analysis uses  $K^-K^+\pi^+$  candidates in a signal region that is within  $\pm 2\sigma_m$  of the fitted  $D_s^+$  mass (SR), where  $\sigma_m$  is the fitted Gaussian width of the  $D_s^+$  peak. Candidates within two symmetric sideband regions (SBR), each of width  $2\sigma_m$  and centered at  $\pm 5\sigma_m$  from the fitted  $D_s^+$  mass, are used to represent the lifetime distribution of background in the SR. The SR and SBR are shown in Fig. 1.

For the lifetime analysis we use the reduced proper time,  $t' = (L - 6\sigma_L)/\beta\gamma c$ . The use of the reduced proper time ensures that only a small acceptance correction to the lifetime distribution is needed [12]. The average proper time resolution for this decay sample (51 fs for Run Period A and 43 fs for Run Period B) is small enough compared to the lifetime to use a binned likeli-

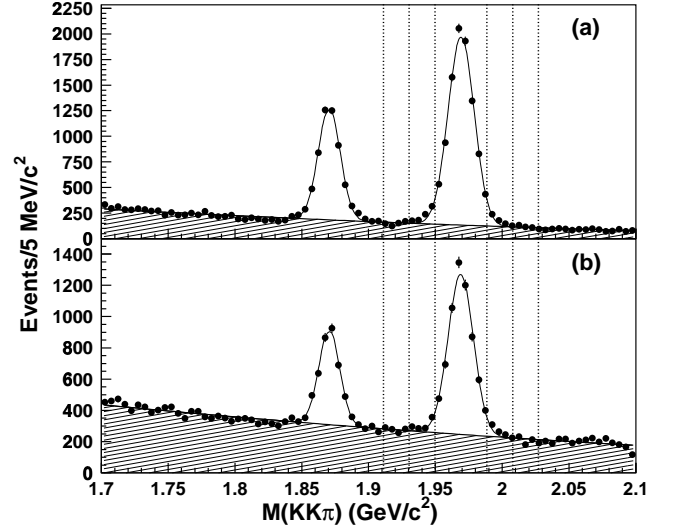


FIG. 1: The  $K^+K^-\pi^+$  invariant mass distributions for the (a)  $\phi(1020)\pi^+$  and (b)  $\bar{K}^*(892)^0 K^+$  decay modes. The data is given by the points while the line gives the fit with the hatched region showing the fitted background level. The vertical dotted lines gives the  $D_s^+$  signal and sideband regions.

hood method. We fit the  $\phi(1020)\pi$  and  $\bar{K}^*(892)^0 K$  decay modes separately. For each decay mode the Run Period A and B data are used in a combined fit.

For each of the run periods A and B, the  $t'$  distributions for the decays in the SR and SBR are binned into two separate histograms from 0–3 ps in 60 fs bins. The observed number of decays in the  $i^{\text{th}}$   $t'$  bin is  $s_i^A$  for the SR and  $b_i^A$  for the SBR, where A refers to Run Period A. The  $t'$  distribution of the SBR is used as a measure of the lifetime distribution of background events in the SR. Thus the expected number of decays ( $n_i(A)$ ) in the  $i^{\text{th}}$   $t'$  bin of the SR for Run Period A is given by:

$$n_i(A) = S_A \frac{f_A(t'_i) e^{-t'_i/\tau}}{\sum_i f_A(t'_i) e^{-t'_i/\tau}} + B_A \frac{b_i^A}{\sum_i b_i^A}, \quad (1)$$

and the likelihood for Run Period A is given by

$$\mathcal{L}_A = \prod_i \frac{n_i(A)^{s_i^A} e^{-n_i(A)}}{s_i^A!} \times \frac{(\alpha_A B_A)^{N_b^A} e^{-\alpha_A B_A}}{N_b^A!}. \quad (2)$$

$S_A$  is the total number of signal events,  $B_A$  is the total number of background events in the SR, and  $S_A + B_A = \Sigma s_i^A$ . The total number of events in the SBR is  $N_b^A = \Sigma b_i^A$  and  $\alpha_A$  is the ratio of the number of events in the SBR to the number of background events in the SR. The value of  $\alpha_A$  is obtained from the fit to the invariant mass distribution and is very close to 1. There is a similar likelihood for Run Period B and the likelihood that is maximized is  $\mathcal{L} = \mathcal{L}_A \times \mathcal{L}_B$ . The fit parameters are  $B_A$ ,  $B_B$ , and  $\tau$ .

The effects of geometrical acceptance, detector, trigger and reconstruction efficiencies, and absorption are

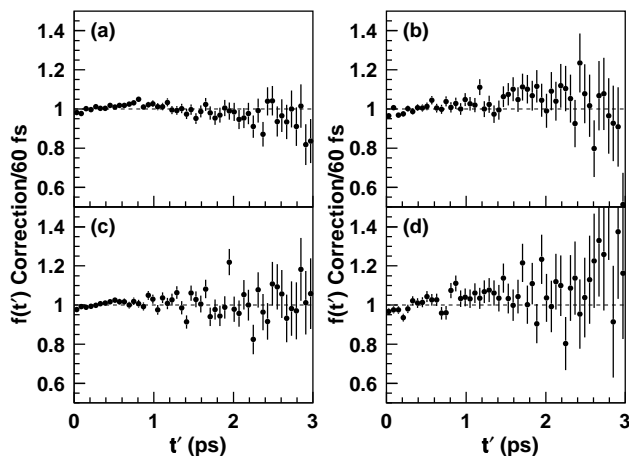


FIG. 2: The  $f(t')$  correction functions for the two decay modes and two run periods (a)  $\phi(1020)\pi$  Run Period B; (b)  $\phi(1020)\pi$  Run Period A; (c)  $\bar{K}^*(892)^0 K$  Run Period B; and (d)  $\bar{K}^*(892)^0 K$  Run Period A. Deviation from a flat line indicates the correction from a pure exponential.

given by the  $f(t')$  correction function. The  $f(t')$  function is determined using a detailed Monte Carlo (MC) simulation of the experiment where the production (using PYTHIA [13]) was tuned so that the production distributions for data and MC matched. A full coherent  $D_s^+ \rightarrow K^- K^+ \pi^+$  decay was simulated using results from FOCUS [14]. The  $f(t')$  distributions are shown in Fig. 2.

We obtain fitted lifetimes of  $507.60 \pm 6.46$  fs and  $506.90 \pm 10.60$  fs for the  $\phi(1020)\pi$  and  $\bar{K}^*(892)^0 K$  decay modes, respectively. The fit confidence levels are 2.0% and 0.13%, respectively. A discussion of these small fit confidence levels is given below. The lifetime distribution of all decays in the SR are shown in Fig. 3 together with the fit and the level of background contained in the SR.

Detailed studies were performed to determine the systematic uncertainty in the lifetime measurement.

The  $f(t')$  correction reduces the fitted lifetime by 0.80%. We studied the uncertainty in this correction. We verified that the MC reproduces the data  $D_s^+$  longitudinal and transverse momenta, the multiplicity of the production vertex,  $\cos\theta^*$ , and the decay length and proper time resolutions. A sensitive check of the acceptance and efficiency part of the MC correction was done using high statistics  $K_S^0 \rightarrow \pi^+ \pi^-$  decays. Short-lived  $K_S^0$  decays were reconstructed using the same analysis methods in the same decay region as the  $D_s^+$  decays. Since the  $K_S^0$  lifetime is well known, we can determine the  $f(t')$  correction in data and compare it to that obtained in our MC simulation. The agreement is excellent but was limited in sensitivity by both data and MC statistics. Using this sensitivity as the level of the uncertainty in the  $f(t')$  correction, we determine a systematic uncertainty due to this correction of  $\pm 0.69\%$ . Possible time dependent systematic effects were looked for by splitting the data into different time periods and comparing the fitted lifetimes.

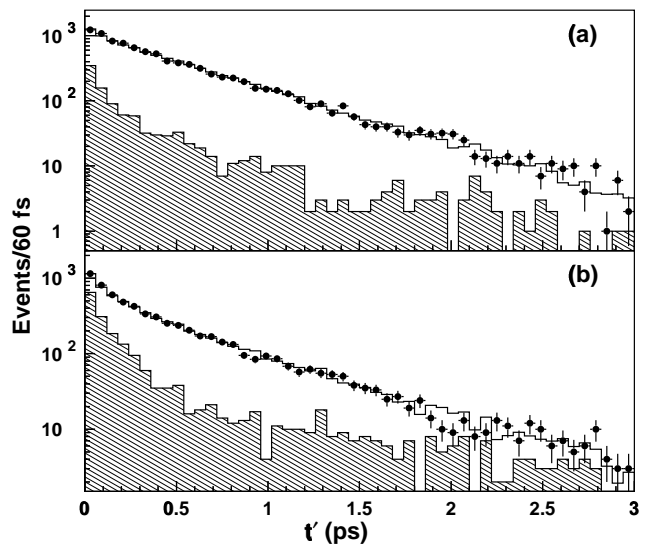


FIG. 3: The lifetime distribution for all decays in the data SR (points), and the fit (histogram). The shaded distribution shows the lifetime distribution of the background component in the SR. The data and fit are shown for Run Periods A and B combined in the same plot for the two decay modes (a)  $\phi(1020)\pi$  and (b)  $\bar{K}^*(892)^0 K$ .

We also compared the separate fitted lifetimes for decays originating from each of the four targets. No systematic uncertainties were found in these comparisons.

Our limited knowledge of the production and decay of the  $D_s^+$  could contribute to a systematic uncertainty. This was studied using different MC simulations where the production parameters and the resonance substructure of the decay were varied over reasonable ranges. Production systematics were also studied by splitting the data into different bins of total and transverse  $D_s^+$  momenta, primary vertex multiplicity, and by comparing the fitted lifetimes for particles and anti-particles. We found no evidence of systematic effects, however, variations of the fitted lifetimes in these studies led us to assign a systematic uncertainty of  $\pm 0.23\%$  due to our limited knowledge of  $D_s^+$  production and decay.

The systematic uncertainty due to absorption of the  $D_s^+$  and daughter particles was determined by varying the  $D_s^+$  interaction cross-section [23] by 100% and the daughter particle interaction cross-sections by 50% in the MC. It was also studied by comparing the lifetimes of decays occurring inside and outside of the target, and by comparing the lifetimes for decays where the  $D_s^+$  was produced in the upstream half of each target with those produced in the downstream half of the same target. We determined a systematic uncertainty of  $\pm 0.38\%$  due to absorption.

In order to use the reduced proper time we must be able to correctly model our proper time resolution. This was verified by comparing the distributions for data and MC and by studying splits of the data sample that can be

sensitive to resolution effects. This included splits in  $t'$  resolution and reconstructed invariant mass and varying the  $t'$  bin width and changing the fitted range for  $t'$ .

The lifetime distribution of the background in the SR is assumed to be well represented by the SBR. The uncertainties that arise because of this assumption were determined by a number of studies.

The contamination from  $D^+ \rightarrow K^- \pi^+ \pi^+$ , and  $\Lambda_c^+ \rightarrow K^- p \pi^+$  decays misidentified as  $K^- K^+ \pi^+$  decays were determined in our sample. As a fraction of the total  $D_s^+ \rightarrow \phi(1020)\pi$  ( $D_s^+ \rightarrow \bar{K}^*(892)^0 K$ ) signal in the SR, we found the above two backgrounds contribute 0.7% (3.0%) and 0.2% (2.5%), respectively. The small contribution of these reflection backgrounds mean they give rise to insignificant uncertainties. This was verified in a test by using stronger particle identification and by explicitly eliminating them by cutting out the appropriate mass regions.

The background lifetime uncertainty was further investigated by using symmetric sidebands of different widths ( $2-4\sigma_m$ ), and located at different separations from the signal region ( $\pm 4$  to  $\pm 6\sigma_m$ ). Variations in particle identification and vertexing selection were used to study the lifetime with changes in the signal/background ratio and this showed no significant effect.

Finally, an independent analysis which did not rely on knowledge of the background lifetime distribution was performed. In this analysis the data were split into fifteen 150 fs wide reduced proper time bins from 0–2.25 ps and one 750 fs wide bin from 2.25–3 ps. The numbers of  $D_s^+ \rightarrow \phi(1020)\pi^+$  and  $\bar{K}^*(892)^0 K^+$  decays in each bin were determined in a mass fit and the yields for the two decay modes separately fitted to an exponential decay distribution modified by a  $f(t')$  correction function. No significant systematic effects were found. To account for the variations of the lifetime in the various background studies we assign a background systematic uncertainty of  $\pm 0.16\%$  ( $\pm 1.09\%$ ) for the  $\phi(1020)\pi$  ( $\bar{K}^*(892)^0 K$ ) decay mode.

A mini-Monte Carlo test of the fit method was done to check the accuracy of the fit errors and to look for possible biases in the fit. We generated 1000 independent data samples from the best fit to the data. Each of these data samples were fit as real data. Distributions of fitted values showed a small bias in the fitted lifetime which is accounted for in a Fit Method systematic uncertainty (see Table I). This study also showed that the fit error underestimates the true statistical uncertainty in the  $\phi(1020)\pi$  ( $\bar{K}^*(892)^0 K$ ) mode by 4.8% (14.7%). The statistical errors on the lifetimes quoted in this paper have been corrected for this effect. These fit properties are due to the background at higher lifetimes and because the  $b_i^{A,B}$  in Eq. (1) are fixed in the fit. The latter also leads to the small reported fit confidence levels. When bin-to-bin fluctuations in the observed  $b_i^{A,B}$  are accounted for in the calculation of the  $\chi^2$ , the fit confidence levels

for  $\phi(1020)\pi$  and  $\bar{K}^*(892)^0 K$  become 8.8% and 16%, respectively. The goodness of fit is further verified by using

TABLE I: Contributions to the systematic uncertainty.

Contribution	Systematic Uncertainty (%)		
	$\phi(1020)\pi$	$\bar{K}^*(892)^0 K$	Combined
Acceptance	$\pm 0.69$	$\pm 0.69$	$\pm 0.69$
Production	$\pm 0.23$	$\pm 0.23$	$\pm 0.23$
Absorption	$\pm 0.38$	$\pm 0.38$	$\pm 0.38$
Backgrounds	$\pm 0.16$	$\pm 1.09$	$\pm 0.41$
Fit Method	$\pm 0.12$	$\pm 1.07$	$\pm 0.38$
Time Scale [15]	$\pm 0.12$	$\pm 0.12$	$\pm 0.12$
Total	$\pm 0.85$	$\pm 1.74$	$\pm 1.00$

TABLE II: Comparison of  $D_s^+$  lifetime measurements and  $\tau(D_s^+)/\tau(D^0)$  ratios. The PDG value of the  $D^0$  lifetime [16] is used in the ratios, except for the FOCUS ratio for which the FOCUS measurement is used [17].

Experiment	$\tau(D_s^+)$ fs	$\tau(D_s^+)/\tau(D^0)$
E687 [18]	$475 \pm 20 \pm 7$	$1.158 \pm 0.052$
E791 [19]	$518 \pm 14 \pm 7$	$1.262 \pm 0.038$
CLEO II.5 [20]	$486.3 \pm 15.0^{+4.9}_{-5.1}$	$1.185 \pm 0.039$
SELEX [21]	$472.5 \pm 17.2 \pm 6.6$	$1.152 \pm 0.045$
FOCUS (this result)	$507.4 \pm 5.5 \pm 5.1$	$1.239 \pm 0.017$

background lifetime distributions taken from fits to the data sideband distributions instead of the actual ( $b_i^{A,B}$ ) entries. This fit method gives consistent lifetimes and fit confidence levels of 9.2% and 18% for  $\phi(1020)\pi$  and  $\bar{K}^*(892)^0 K$ , respectively.

We have measured the  $D_s^+$  lifetime to be  $507.4 \pm 5.5$  (stat.)  $\pm 5.1$  (syst.) fs using  $8961 \pm 105$   $D_s^+ \rightarrow \phi(1020)\pi^+$  and  $4680 \pm 90$   $D_s^+ \rightarrow \bar{K}^*(892)^0 K^+$  decays from the Fermilab FOCUS photoproduction experiment. We also determined the ratio of our  $D_s^+$  lifetime to our  $D^0$  lifetime [17] to be  $1.239 \pm 0.014$  (stat.)  $\pm 0.009$  (syst.), where the systematic uncertainty in the ratio is reduced by eliminating common systematic contributions. Table II compares our measurement with recent published results. This measurement represents a significant improvement in precision.

We wish to acknowledge the assistance of the staffs of Fermi National Accelerator Laboratory, the INFN of Italy, and the physics departments of the collaborating institutions. This research was supported in part by the U. S. National Science Foundation, the U. S. Department of Energy, the Italian Istituto Nazionale di Fisica Nucleare and Ministero dell'Istruzione, dell'Università e della Ricerca, the Brazilian Conselho Nacional de Desenvolvimento Científico e Tecnológico, CONACyT-México, the Korean Ministry of Education, and the Korean Science and Engineering Foundation.

- 
- [1] G. Bellini, I. I. Bigi, and P. J. Dornan, Phys. Rept. **289**, 1 (1997).
  - [2] S. Bianco, F. L. Frabbi, D. Benson, and I. Bigi, Riv. Nuovo Cim. **26N7**, 1 (2003).
  - [3] I. I. Bigi and N. G. Uraltsev, Z. Physik **C62**, 623 (1994).
  - [4] H. W. K. Cheung, JHEP PRHEP-hf8/022, FERMILAB-CONF-99-344, hep-ex/9912021.
  - [5] S. Nussinov and M. V. Purohit, Phys. Rev. **D65**, 034018 (2002).
  - [6] I. I. Bigi, hep-ph/0112155.
  - [7] I. I. Bigi and N. G. Uraltsev, Nucl. Phys. **B423**, 33 (1994).
  - [8] I. I. Bigi, M. A. Shifman, and N. Uraltsev, Ann. Rev. Nucl. Part. Sci. **47**, 591 (1997).
  - [9] P. L. Frabetti *et al.*, Nucl. Instrum. Methods Phys. Res., Sect. A **320**, 519 (1992).
  - [10] J. M. Link *et al.*, Nucl. Instrum. Methods Phys. Res., Sect. A **516**, 364 (2004).
  - [11] J. M. Link *et al.*, Nucl. Instrum. Methods Phys. Res., Sect. A **484**, 270 (2002).
  - [12] H. W. K. Cheung, AIP Conf. Proc. **618**, 321 (2002), hep-ex/0111050.
  - [13] T. Sjöstrand *et al.*, Comput. Phys. Commun. **135**, 238 (2001).
  - [14] S. Malvezzi, AIP Conf. Proc. **549**, 569 (2002).
  - [15] J. M. Link *et al.*, Phys. Rev. Lett. **88**, 161801 (2002).
  - [16] S. Eidelman *et al.*, Phys. Lett. **B592**, 1 (2004).
  - [17] J. M. Link *et al.*, Phys. Lett. **B537**, 192 (2002).
  - [18] P. L. Frabetti *et al.*, Phys. Rev. Lett. **71**, 827 (1993).
  - [19] E. M. Aitala *et al.*, Phys. Lett. **B445**, 449 (1999).
  - [20] G. Bonvicini *et al.*, Phys. Rev. Lett. **82**, 4586 (1999).
  - [21] M. Iori *et al.*, Phys. Lett. **B523**, 22 (2001).
  - [22] The charge conjugate mode is implicitly implied unless otherwise stated.
  - [23] The  $D_s^+$  cross section is taken to be half the neutron cross section.